DEVELOPMENT OF A FULLY INKJET PRINTED ANTENNA ON POLYETHYLENE TEREPHTHALATE FOR ENERGY HARVESTING PURPOSES IN SMART LABELLING

W. A. I. B. J. Wickramasinghe[a], S. W. D. K. R. M. Manamendra, W. L. P. K. Wijesinghe, G. C. Wickramasinghe, D. L. Weerawarne*

Department of Physics, Faculty of Science, University of Colombo, Sri Lanka

[a]*isurubhathiya1998@gmail.com*

**dweerawa@phys.cmb.ac.lk*

1. ABSTRACT

Flexible printed electronics offer a revolutionary approach to smart labelling. However, achieving energy autonomy remains a critical hurdle. While passive Near Field Communication (NFC) enables battery-free operation via electromagnetic energy harvesting, peak performance necessitates precise resonance around 13.56 MHz. This study investigates the fabrication of single-sided flexible antenna using inkjet printing by a regular office inkjet-printer, specifically addressing the usefulness of such printers in electronics fabrication and addressing the geometric deviations inherent in the process. Analysis of silver (Ag) nanoparticle conductive traces printed on polyethylene terephthalate (PET) substrate revealed that line-width deviations are highly dependent on motion of the print-head orientation. To mitigate this, a directional compensation strategy was developed to offset fabrication deviations during the digital design phase. The optimized single-layer antenna on PET achieved a harvested voltage of 3.220 ± 0.001 V, comparable to a standard rigid PCB antenna, yet exhibited a high series resistance of 583.2 ± 0.1 Ω with a low Q-factor. To overcome these limitations, a multilayer printing technique was implemented. The resulting three-layer inkjet-printed Ag antenna on PET reduced series resistance to 190.5 ± 0.1 Ω and increased harvested voltage to 3.250 ± 0.001 V with higher resonance characteristics. These results demonstrate that geometrically compensated, multilayer inkjet-printed antennas on PET substrates can achieve the electrical performance necessary for reliable, battery-free smart labelling in high-impedance, low-power sensing applications.

Keywords: Inkjet Printing, Near Field Communication, Energy Harvesting, Smart Labelling

2. INTRODUCTION

Printed electronics enables the development of "smart labels" for packaging by creating circuits on a flexible substrate [1], [2]. To achieve energy autonomy, these devices often utilize Passive Near Field Communication (NFC) to harvest energy from electromagnetic fields [3], [4]. However, efficient harvesting requires the antenna to resonate at 13.56 MHz, which depends critically on the geometric accuracy of the printed inductance [5]. This poses a significant challenge for inkjet printing, particularly when using general purpose office inkjet printers. Unlike the subtractive etching processes used for rigid PCBs, inkjet printing is an additive process susceptible to ink spreading and geometric anisotropy [6]. This anisotropy arises because deposition accuracy is governed by the line's orientation relative to the print head's scanning axis. While lines parallel to the head motion (0°) are deposited continuously, lines perpendicular to this motion (90°) are constructed via rasterized segments or discontinuous

firing. This mechanical difference causes deviation to increase as the print angle diverges from the scanning axis, significantly altering the antenna's impedance and resonant frequency.

This aims to establish the suitability of regular office inkjet printer in fabricating electronics and quantifies geometric deviations on PET substrate to develop a directional compensation strategy that offsets fabrication deviations in the digital design phase. We validate this approach by comparing the resonance quality and energy harvesting voltage of the optimized flexible antenna against single sided PCB antenna.

3. THEORY

Series LCR Resonance frequency, Inductance and Q-Factor

Resonance occurs in an LC circuit when the inductive reactance ($XL = 2\pi fL$) equals the capacitive reactance ($X_C = 1/2\pi fC$). At this point, denoted as the resonant frequency (f_0) in Equation 1, the circuit oscillates at its natural frequency determined by its inductance and capacitance:

$$f_0 = \frac{1}{2\pi\sqrt{LC}} \qquad (1)$$

The energy in the circuit swings between the inductor and the capacitor. Ideally, if there were no resistive losses, the energy would oscillate indefinitely. Real circuits, however, have inherent resistance that dissipates energy, damping the oscillations over time.

Ideally, the NFC antenna functions as a lossless LC tank circuit oscillating at $f_{res} = 13.56\,MHz$. However, printed antennas possess significant internal resistance, effectively forming a series LCR circuit. The quality factor (Q-factor) in Equation 2 of such a system, which defines the sharpness of the resonance peak and the efficiency of energy storage, is given by:

$$Q = \frac{1}{R}\sqrt{\frac{L}{C}} \qquad (2)$$

where R is the total series resistance, L is the equivalent inductance, and C is the tuning capacitance. As indicated by the equation, the Q-factor is inversely proportional to resistance. Consequently, antennas with high internal resistance exhibit a low Q-factor, resulting in rapid energy dissipation and a broad, shallow resonance curve (S11) that may be difficult to detect via inductive coupling methods.

Antennas operating at 13.56 MHz which are used for NFC communication, can be designed in various forms for different application needs. The focus of this study is solely on square-shaped antennas. One of the crucial parameters for these antennas is the equivalent inductance (L) of the antenna. Therefore, the Inductance of squared antennas can be calculated using the Equation 3 according to their physical dimensions.

$$L_{ant} = K_1 \cdot \mu_0 \cdot N^2 \cdot \left[\frac{\frac{d_{out} + d_{in}}{2}}{1 + K_2 \cdot \left(\frac{d_{out} - d_{in}}{d_{out} + d_{in}} \right)} \right] \quad (3)$$

$\mathbf{K_1}$ = 2.34
$\mathbf{K_2}$ = 2.75
$\boldsymbol{\mu_0}$ = $4\pi \times 10^{-7}$ H/m
$\mathbf{N}$ = number of turns
$\mathbf{d_{out}}$ = outer diameter of the antenna
$\mathbf{d_{in}}$ = inner diameter of the antenna
$\mathbf{L_{ant}}$ = self-inductance of the loop antenna measured in Henry at 13.56 MHz

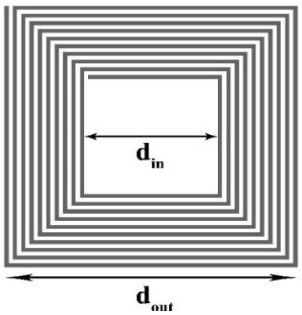

Figure 1: Physical dimensions of a square antenna taken into account to calculate self - inductance.

4. METHODOLOGY AND INSTRUMENTATION

a. Development of Near Field Communication (NFC) antenna

The antenna design began by identifying the internal tuning capacitance of the M24LR04E-R IC, which was determined to be 27.5 pF from the datasheet [7]. Subsequently, following the guidelines in the application note and applying the resonant frequency formula in Equation 1 for 13.56 MHz, the essential equivalent inductance for the antenna was calculated to be 5.0 μH. An antenna with an approximate inductance of 5.0 μH was designed utilizing the eDesignSuite [8], [9]. This online tool, developed by STMicroelectronics NV, facilitates the creation of NFC antenna designs tailored to specific requirements. Utilizing this tool is a more time-efficient option than manually calculating antenna dimensions using the Equation (3). However, the tool estimates equivalent inductance based on rigid PCB parameters and corrections were essential for flexible materials due to inductance differences. The antenna designed via eDesignSuite featured dimensions of 42 mm × 42 mm with eleven turns, a conductor width of 0.6 mm, and a spacing of 0.6 mm as shown in Figure 2. To enhance practicality for printing and connectivity, the design was further refined using Inkscape to incorporate modifications such as soldering pads.

Development of the flexible antenna on the PET substrate was done by using an office inkjet printer and the performance was compared to a rigid PCB antenna. The microprocessor M24LR04E-R was used for energy harvesting through NFC communication capabilities [7]. The circuit was designed without an onboard antenna and with the ability to connect antennas externally. The circuit was configured using the "M24LR.h" Arduino library to enable its energy harvesting mode. Following fabrication, the firmware required for NFC communication and energy harvesting was uploaded to the custom board via an Arduino UNO.

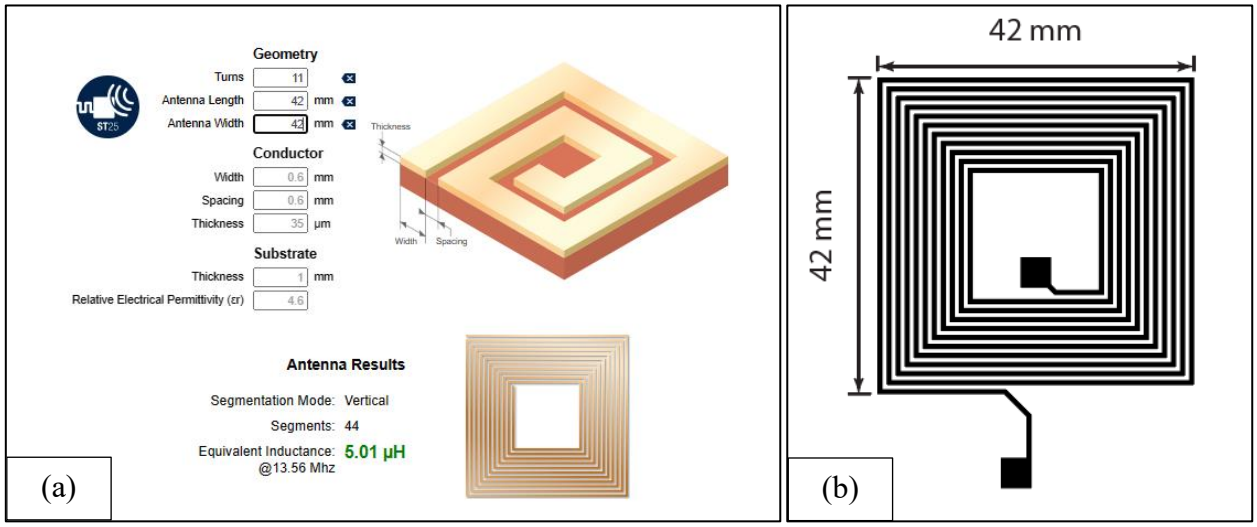

Figure 2: **(a)** interface of eDesign suit with the proposed antenna design and **(b)** proposed NFC antenna design after enhancing using Inkscape.

i. Fabrication of single-side rigid antenna

The antenna was fabricated as-designed on a rigid PCB, and its inductance was measured using a Keysight Technologies U1731C LCR meter at 100 kHz, the maximum frequency setting available on the device. Afterwards, the antenna was connected to the previously developed circuit to evaluate its NFC functionality and energy harvesting performance. To verify NFC communication, a test data string was written to the board's memory via the firmware. An NFC-enabled mobile phone (Nokia 6.1) served as both the electromagnetic energy source and the NFC reader. The test string was successfully retrieved by the phone to confirm connectivity, while the maximum harvested voltage output from the board was measured using a multimeter. Finally, the antenna's return loss curve (S_{11}) was assessed using an AURSINC-manufactured NanoVNA (Nano Vector Network Analyzer).

ii. Fabrication of single-side flexible antenna

Achieving precise geometric dimensions is crucial for fabrication an NFC flexible antenna on a PET substrate. However, inkjet printing, the actual dimensions of the printed lines often deviate from the intended design, particularly with a domestic printer. This deviation is primarily attributed to printer characteristics and the orientation of the lines relative to the print head's motion [10]. To investigate the impact of print orientation on this deviation, the following methodology was employed.

4.1.2.1 Microscopic analysis of inkjet printed lines

To investigate dimensional deviation in inkjet-printed NFC antenna patterns, test coupons in Figure 3 (a) were designed using Inkscape software. The design featured conductive lines with intended widths and separation gaps as 0.9 mm, 0.6 mm, and 0.3 mm. The test coupon in Figure 3 (a) was printed using an EPSON L130 printer with NovaCentrix Metalon® JS-B25P silver nanoparticle ink on NovaCentrix: Novele™ IJ-220 PET. The coupons were printed at orientation angles ranging from 0° to 180° in 18° increments relative to the print head motion. After printing, these lines on PET were sintered at 110 °C for four hours.

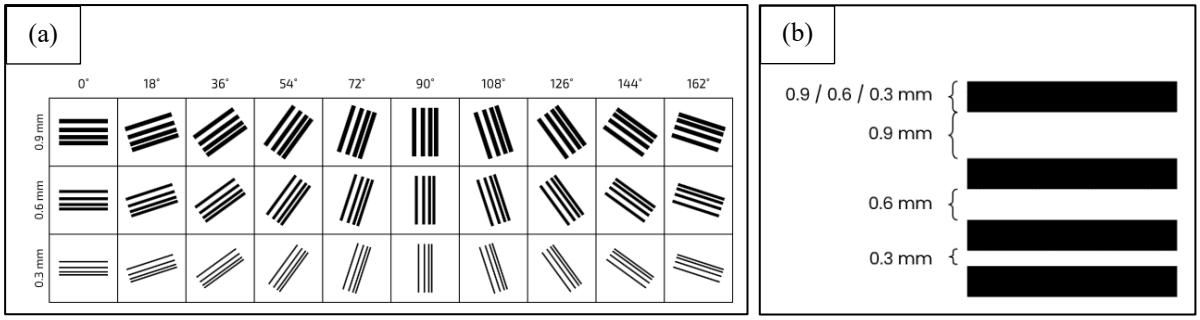

Figure 3: **(a)** The test coupon design that use for line analysis and **(b)** dimensions of single cell of the test coupon

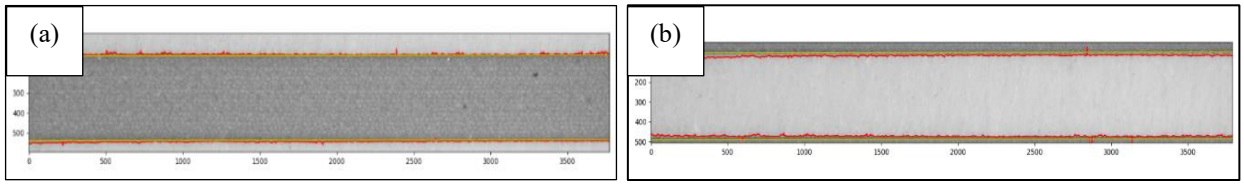

Figure 4: **(a)** Detecting edges of the printed lines using python script and **(b)** detecting edges of the printed line and gaps using python script.

The printed lines in shown in figure 4 were imaged using an ANDONSTAR AD 249s digital microscope with a calibration scale. Analysis of these images was performed using a custom Python script that used Otsu's thresholding method to separate the printed lines from the background. The script calculated the mean width and standard deviation of the lines by measuring the pixel width at every position along the line length.

Subsequent antenna designs were adapted for PET based on the deviation data obtained from the above line analysis phase, including the design fabricated on a rigid PCB. Three designs in table 1 were fabricated on PET, using silver ink by EPSON L130 printer and sintered under 110 °C for 4 hours.

The design 1 on PET showed resistance of 516.5 ± 0.1 Ω. Inductance measurements taken (Keysight U1731C) revealed discrepancies between the simulated and actual values. While, interfaced with the NFC circuit, this flexible antenna failed to achieve successful communication, likely due to inductance mismatches caused by substrate flexibility and ink spreading. To address this, two additional single - side antennas of design 2 and design 3 were developed with adjusted inductances and dimensions according to the dimensions in Table 1.

Table 1 - dimensions of the antenna designs (The following dimensions were adjusted in the vector file according to the results obtained in the 'Inkjet Printed Line Analysis' phase).

Design No.	Size (mm × mm)	Turns (N)	Trace Width (mm)	Spacing (mm)	Est. Inductance (µH)
1	42 × 42	11	0.6	0.6	5.01
2	40 × 40	14	0.4	0.4	9.12
3	33 × 33	15	0.3	0.3	8.61

Then all these antennas were connected to a custom PCB that was designed and evaluated for NFC communication using a mobile phone, and maximum harvested voltage outputs were measured using a multimeter. Then, the return loss curves were observed using NanoVNA.

Based on the results from the above experiment, it was necessary to identify a method to reduce the internal resistance of the antennas fabricated on PET. One potential solution to achieve this is printing multiple conductive layers on the same trace. Consequently, a three-layer version of Antenna Design 2 was fabricated, and its internal resistance and performance were evaluated following the experimental procedure described above.

5. RESULTS AND DISCUSSION

a. Geometric Deviation Analysis

To quantify fabrication tolerances, conductive lines were printed on PET at orientation angles ranging from 0° (parallel to print head motion) to 180°. Microscopic analysis revealed a significant correlation between print orientation and dimensional accuracy; specifically, the results showed minimum deviation from the expected dimensions at 0° (and 180°) and maximum deviation at 90°.

Visual Inspection: Lines printed at 0°, as indicated in Figure 5(a), exhibited smooth, well-defined edges. In contrast, lines printed at 90° shown in Figure 5(b) increased roughness and ink dispersion perpendicular to the print direction.

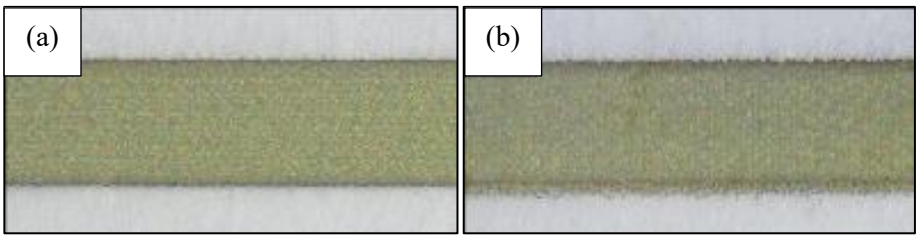

Figure 5: Microscopic image of silver lines **(a)** printed line with 0° angle relative to the motion of the printer head on PET and **(b)** printed line with 90° angle relative to the motion of the

Quantitative Deviation: Image analysis (using the Otsu thresholding method) confirmed that dimensional deviation peaks when lines are printed perpendicular to the print head motion. Table 2 illustrates the variations of the lines widths and gaps vary as following ranges for PET. However, these deviation values were independent from the target line widths and gaps values.

Table 2 - Measured maximum geometric deviations for printed lines and separation gaps at 0° and 90° angles

Substrate	**Target Line Widths (mm)**	**Max Width Increase at 0° (mm) ± 0.005 mm**	**Max Gap Reduction at 0°(mm) ± 0.005 mm**	**Max width Increase at 90° (mm) ± 0.01 mm**	**Max Gap Reduction at 90° (mm) ± 0.01 mm**
PET	0.3, 0.6, 0.9	From + 0.040 to + 0.050	From - 0.042 to - 0.085	From +0.10 to +0.12	From -0.12 to -0.18

Design Compensation Strategy: Based on these results, a compensation factor was applied to the digital designs. For example, to achieve a target trace width of 0.9 mm in a vertical (90°) orientation on PET, the digital design was pre-compensated to 0.79 mm (0.9 mm - 0.11 mm offset). This calibration ensured that the final antenna dimensions matched the inductive requirements for resonance at 13.56 MHz.

Table 3 - Design compensation factors applied to counteract ink spreading.

Substrate	**Compensation Factor Applied for width at 0° (mm)**	**Compensation Factor Applied for gap at 0° (mm)**	**Compensation Factor Applied for width at 90° (mm)**	**Compensation Factor Applied for gap at 90° (mm)**
PET	- 0.045	+ 0.064	- 0.11	+ 0.15

b. Flexible antenna performance analysis

The electrical characteristics and NFC performance of the three single-sided antenna designs fabricated on PET are summarized in Table 4. Further, the single side rigid PCB antenna performance was compared with antennas on PET.

Table 4 - key parameters and the performances of the antenna designs

Substrate	PCB	PET			
	Design 1 (1 layer)	Design 1 (1 layer)	Design 2 (1 layer)	Design 2 (3 layers)	Design 3 (1 layer)
Est. Inductance from the eDesign suit at 13.56 MHz (μH)	5.01	5.01	9.12	9.12	8.61
Actual Inductance (μH)	4.82 ± 0.01	3.00 ± 0.01	6.20 ± 0.01	6.20 ± 0.01	5.20 ± 0.01
Antenna resistance (Ω)	3.387 ± 0.001	516.5 ± 0.1	583.2 ± 0.1	190.5 ± 0.1	752.7 ± 0.1
Maximum voltage of the harvested energy (V)	3.255 ± 0.001	0.048 ± 0.001	3.220 ± 0.001	3.250 ± 0.001	2.575 ± 0.001
NFC communication compatibility	Yes	No	Yes	Yes	Yes

The flexible antennas fabricated on PET demonstrated functional inductance values (6.20 μH), while bit higher than the target, remained within the tuning range of the M24LR04E-R IC when combined with its internal capacitance and significantly higher resistance (~ 500 – 750 Ω). Consequently, designs 2 and 3 on PET supported NFC communication. Notably, Design 2 achieved a harvested voltage of 3.220 V, which is comparable to the reference rigid PCB (3.25 V). However, the resistance still remained significantly high relatively to PCB antenna, resulting in a low Q-factor. To address this, a three-layer version of Design 2 was fabricated on PET. This modification reduced the resistance by approximately a factor of three, from 583.2 ± 0.1 Ω to 190.5 ± 0.1 Ω, while achieving a comparable harvested voltage of 3.250 V.

Return Loss (S_{11}) Analysis: Figure 6 show the return loss curves for the copper PCB antennas with distinct resonance dips around 13.56 MHz. However, the flexible antenna (Design 2) lacks this distinct dip despite functional NFC coupling. This is attributed to the antenna's relatively high series resistance (≈ 583 Ω), which drastically lowers the Q-factor of the LC circuit [11], [12]. The low Q-factor broadens the resonance peak, making the power absorption dip indistinguishable during non-contact measurements, even though sufficient energy transfer occurs for device operation. However, the three-layer flexible antenna (Design 2) exhibits a shallow and broad, yet observable, dip in the curve. This indicates that the reduced internal resistance of the multilayer antenna (≈ 190 Ω) has increased the Q-factor of the LC circuit.

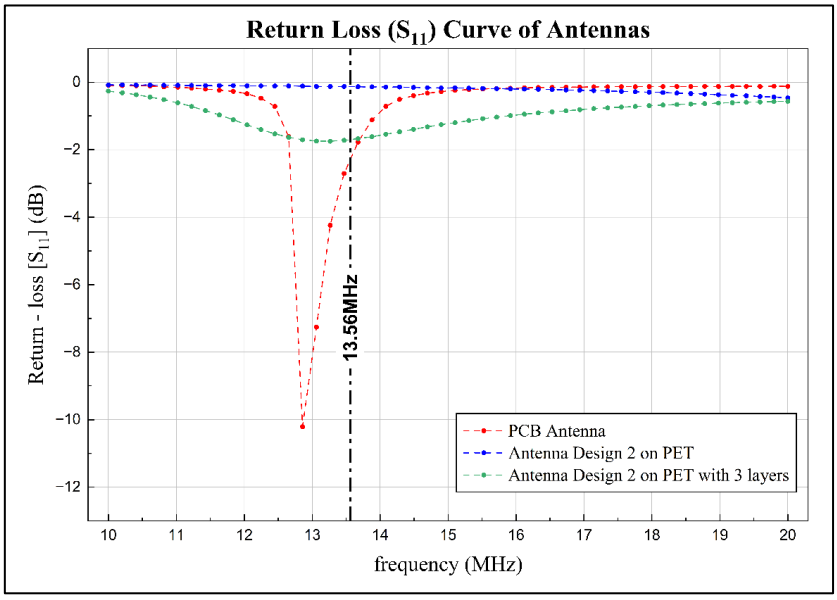

Figure 6: Return-Loss (S_{11}) curves of the fabricated antennas

6. CONCLUSION

The study successfully characterized and optimized inkjet-printed NFC antennas on PET. Geometric analysis revealed significant anisotropy, with conductive lines widening by up to 0.12 mm at a 90° print orientation while remaining relatively accurate at 0°. By implementing a directional compensation strategy, specifically reducing vertical trace widths in the digital design, we achieved the geometric precision required for resonance around 13.56 MHz for antenna on PET. The reference rigid PCBs established a voltage benchmark of 3.25 – 3.33 V, the optimized flexible antenna (Design 2 on PET) achieved a comparable 3.220 ± 0.001 V. Crucially, despite inherent material challenges, the flexible antenna successfully established reliable NFC communication with the reader, validating the design's functionality. However, a trade-off was observed between voltage generation and power delivery. The single-layer flexible antenna on PET exhibited a shallower return loss S11 dip compared to its rigid counterparts. This is attributed to the high series resistance (583.2 ± 0.1 Ω), which lowers the circuit's Q-factor and limits current sourcing capability due to ohmic losses. To address this, multilayer printing was explored as a solution. A three-layer version of the antenna design 2 fabricated on PET demonstrated much more performance improvements. This approach reduced the series resistance by a factor of three (to 190.5 ± 0.1 Ω) compared to the single-layer counterpart, thereby increasing the antenna's Q-factor. This improvement was evidenced by a shallow and broad but distinct dip in the return loss curve around the NFC resonance frequency. In conclusion, this work demonstrates that inkjet-printed antennas fabricated by regular desktop inkjet printer are viable alternatives to rigid PCBs for high-impedance, low-power sensing nodes. Future work should focus on further reducing trace resistance to support current-intensive loads. This could be achieved by refining multilayer alignment techniques to allow for higher layer counts or by investigating alternative inks with inherently lower resistivity to enhance radiation efficiency.

7. REFERENCES

[1] C. Yue, J. Wang, Z. Wang, B. Kong, and G. Wang, "Flexible printed electronics and their applications in food quality monitoring and intelligent food packaging: Recent advances," *Food Control*, vol. 154, p. 109983, Dec. 2023, doi: 10.1016/j.foodcont.2023.109983.

[2] S. Tripathi, S. Bisht, P. Kumar, Md. R. Mia, and K. K. Gaikwad, "Printable and flexible electronics for smart packaging applications: status, challenges, and opportunities," *Journal of Materials Science: Materials in Electronics*, vol. 36, no. 25, p. 1583, Sep. 2025, doi: 10.1007/s10854-025-15626-w.

[3] H. Kang *et al.*, "Fully roll-to-roll gravure printable wireless (13.56 MHz) sensor-signage tags for smart packaging," *Sci. Rep.*, vol. 4, Jun. 2014, doi: 10.1038/srep05387.

[4] C. L. Baumbauer *et al.*, "Printed, flexible, compact UHF-RFID sensor tags enabled by hybrid electronics," *Sci. Rep.*, vol. 10, no. 1, p. 16543, Oct. 2020, doi: 10.1038/s41598-020-73471-9.

[5] Q.-T. Luu, S. Koulouridis, A. Diet, Y. Le Bihan, and L. Pichon, "Investigation of inductive and radiating energy harvesting for an implanted biotelemetry antenna," in *2017 11th European Conference on Antennas and Propagation (EUCAP)*, Paris: IEEE, Mar. 2017, pp. 160–163. doi: 10.23919/EuCAP.2017.7928620.

[6] R. Vyas *et al.*, "Inkjet printed, self powered, wireless sensors for environmental, gas, and authentication-based sensing," *IEEE Sens. J.*, vol. 11, no. 12, pp. 3139–3152, 2011

[7] STMicroelectronics, "M24LR04E-R: Dynamic NFC/RFID tag IC with 4-Kbit EEPROM, energy harvesting, I2C bus and ISO 15693 RF interface," 2017. Accessed: Jan. 23, 2026. [Online]. Available: https://www.st.com/resource/en/datasheet/m24lr04e-r.pdf

[8] STMicroelectronics, "Application Note - How to design a 13.56 MHz customized antenna for ST25 NFC / RFID Tags," no. AN2866, Rev. 5, Aug. 2021, Accessed: Jan. 23, 2026. [Online]. Available: https://www.st.com/resource/en/application_note/an2866.pdf

[9] STMicroelectronics, "NFC Inductance Calculator - eDesignSuite." Accessed: Jan. 23, 2026. [Online]. Available: https://eds.st.com/antenna/#/

[10] C. Buga and J. C. Viana, "Inkjet Printing of Functional Inks for Smart Products," in *Production Engineering and Robust Control*, IntechOpen, 2022. doi: 10.5772/intechopen.104529.

[11] Ralph Jacobi and Eddie LaCost, "Antenna Design Guide for the TRF79xxA," 2017. Accessed: Jan. 15, 2026. [Online]. Available: https://www.ti.com/lit/an/sloa241b/sloa241b.pdf

[12] NXP Semiconductors, "AN13219 PN7160 antenna design and matching guide Rev. 1.5-27 February 2024 Application note Document information Information Content PN7160 antenna design and matching guide," 2024. Accessed: Jan. 15, 2026. [Online]. Available: https://www.nxp.com/docs/en/application-note/AN13219.pdf